

# Self-Assembled Iron Oxide Nanoparticle-Modified APTES-ITO Electrode for Simultaneous Stripping Analysis of Cd(II) and Pb(II) Ions

Noorhashimah Mohamad Nor, Sarasijah Arivalakan, Nor Dyana Zakaria, Nithiyaa Nilamani, Zainovia Lockman, and Khairunisak Abdul Razak\*



Cite This: *ACS Omega* 2022, 7, 3823–3833



Read Online

ACCESS |



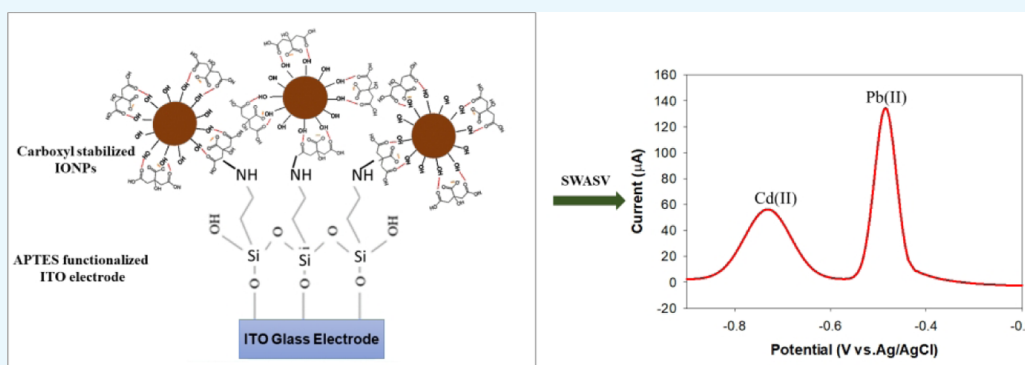
Metrics & More



Article Recommendations



Supporting Information



**ABSTRACT:** Carboxyl (–COOH)-stabilized iron oxide nanoparticles (IONPs) synthesized through co-precipitation were used to modify an indium tin oxide (ITO) electrode, which was chemically functionalized with 3-aminopropyltriethoxysilane (APTES) for heavy metal detection. The effect of soaking time (30, 60, 90, and 120 min) of IONP-COOH self-assembled on an APTES-ITO electrode was studied. Cyclic voltammetry and scanning electron microscopy were applied to analyze the electrochemical properties and morphologies of IONP-COOH/APTES-ITO modified electrode. The modified electrodes were then employed for the simultaneous detection of Cd(II) and Pb(II) by using square wave anodic stripping voltammetry. At 90 min of soaking time, excellent electrochemical performance and larger effective surface area ( $A_e$ ) were obtained. The linear range for the simultaneous detection of Cd(II) and Pb(II) ions using the modified electrode was 10–100 ppb with limits of detection of 0.90 and 0.60 ppb, respectively. The interference study revealed a low interference effect from Cr(III), Hg(II), Zn(II), Cu(II), Mg(II), Na(I), and K(I) toward the simultaneous detection of Cd(II) and Pb(II). Finally, the IONP-COOH/APTES-ITO-modified electrode was applied to analyze seawater samples and was able to simultaneously detect Cd(II) and Pb(II) ions.

## 1. INTRODUCTION

Heavy metal pollution is a global problem that has attracted public interest due to their health effects. The term heavy metal is defined as chemical elements with an atomic weight between 63.5 and 200.6 and metal density greater than 5 g/cm<sup>3</sup>.<sup>1</sup> Although heavy metal ions exist in nature (volcanic activity), their contamination is mainly caused by anthropic (manmade) activities such as industrialization, urbanization, and agriculture. The bioavailability, mobility, and toxicity of heavy metals depend on their specific chemical form or binding that can be changed by several physical and chemical factors, such as pH, temperature, redox potential, and organic ligand concentrations. These factors can convert heavy metals from a solid phase to a liquid phase and sometimes cause the pollution of surrounding water bodies. The most commonly found heavy metals in wastewater effluents are arsenic (As),

cadmium (Cd), chromium (Cr), copper (Cu), lead (Pb), mercury (Hg), nickel (Ni), silver (Ag), and zinc (Zn).<sup>2</sup>

Frequent exposure to these heavy metals, either directly (workplace) or indirectly (ingestion of contaminated food and water), can cause severe health issues. Therefore, the concentration of heavy metal in the environment must be monitored. Inductively coupled plasma-optical emission spectrometry (ICP-OES), inductively coupled plasma-mass spectrometry (ICP-MS), and atomic absorption spectrometry

**Received:** December 19, 2021

**Accepted:** January 11, 2022

**Published:** January 19, 2022



(AAS) are widely used to detect the presence of heavy metals and their concentration. Although these techniques are highly sensitive, they require skilled personnel, have time-consuming sample preparation and analysis, and high costs. Therefore, a low-cost, simple, and highly sensitive analytical technique based on optical sensor and electrochemical sensor systems must be developed for heavy metal detection.<sup>3</sup> Some of the analytical techniques that use optical sensors include plasmonic, fluorescence, and surface enhancement Raman scattering (SER). Optical sensors utilize electromagnetic radiation to generate an analytical signal in a transduction unit. Interactions between the radiation and the sample are measured as changes in a specific optical parameter, which represents the analyte concentration.<sup>4</sup> The limitations of optical sensors are unspecific molecular probes and high cost.

Electrochemical sensing has been studied for heavy metal detection due to its simplicity, low cost, excellent sensitivity, and low limit of detection (LOD). This technique does not require any molecular recognition probe on the bare electrode because the speciation toward specific heavy metal can be attained through the electrocatalytic oxidation of pre-concentrated heavy metal ions on the electrode surface.<sup>5</sup> However, the sensor performance is dependent on the reaction between the working electrode and the solution interface. Thus, the surface structure and types of working electrode materials are crucial factors in determining the rate of the electrochemical reaction. Working electrodes have been modified with nanomaterials such as gold, bismuth, graphene oxide, and iron oxide to improve the sensitivity, specificity, and LOD of the working electrode in heavy metal detection.<sup>6–8</sup>

Owing to their catalytic properties, high affinity toward heavy metal ions, less toxicity, and chemical stability, iron oxide nanoparticles (IONPs) have been widely used to modify working electrodes to detect heavy metals at a low detection limit.<sup>9–11</sup> Lee et al. (2016)<sup>12</sup> reported that the electrochemical detection of Zn(II), Cd(II), and Pb(II) using *in situ* bismuth plating and IONP/graphene/glass carbon electrode (GCE) have LODs of 0.11, 0.08, and 0.07 ppb, respectively. The modified electrode showed high sensitivity for heavy metal ion detection due to the combination of the good electrical conductivity of graphene and the good catalytic properties of IONPs. Maleki et al. (2019)<sup>13</sup> reported the simultaneous detection of Cd(II) and Pb(II) by using the modified magnetic carbon paste electrode (MCPE) with polyamidoamine dendrimer-functionalized magnetic nanoparticles. Low LODs of 0.21 and 0.17 ppb were obtained for Cd(II) and Pb(II), respectively. The modified electrode showed excellent performance because the polyamidoamine dendrimer provided a high surface area binding site for the absorption of heavy metal ions on the electrode surface. Wu et al. (2019)<sup>14</sup> used an IONP/fluorinated multiwalled carbon nanotube (MWCNT)/GCE-modified electrode and achieved high sensitivity and simultaneous detection of Cd(II), Pb(II), Cu(II), and Hg(II) with LODs of 0.05, 0.08, 0.02, and 0.05 nM, respectively. The excellent electrochemical performance was attributed to the strong negative charge of the semi-ionic C–F bond present on the fluorinated-MWCNT and the synergistic interaction of IONPs with fluorinated MWCNTs.

However, most of the reported works for the IONP-modified electrode for simultaneous heavy metal detection used carbon-based electrodes, such as a glassy carbon electrode<sup>7,15,16</sup> and carbon paste electrode.<sup>8,17</sup> However, these electrodes are excessively large for *in situ* measurement,

not portable, and require tedious electrode preparation for modification with nanomaterials. The disposable electrodes, such as a screen-printed carbon electrode (SPCE) and indium tin oxide (ITO) electrode, are small, portable, and can be mass produced at low costs.<sup>18</sup> SPCEs have been modified with nanoparticles to increase their sensitivity and selectivity for heavy metal detection.<sup>6,19,20</sup> Only limited studies have been conducted with nanoparticle-modified ITO as the working electrode for heavy metal detection. ITO electrodes offer excellent electrical conductivity, a smooth surface, low cost, good electrochemical properties, and good substrate adhesion. Some of the reported works<sup>14,21</sup> obtained excellent electrochemical performance for heavy metal detection by using the combination of IONPs with other nanomaterials forming a hybrid or nanocomposite-modified electrode. However, additional synthesis processes and more investigation parameters were required. Therefore, simple, high sensitivity, low LOD, and high reproducibility IONP-modified ITO electrodes for portable heavy metal detection are in demand.

In addition, most reported works on IONP-modified electrodes were fabricated using a drop-casting technique due to its simple process and ability to control the amount of IONPs adsorbed on the electrode. However, the main challenge of drop-casting IONPs to modify an ITO electrode is the tendency of the IONP layer to peel off after electrochemical analysis or repeated washing due to the weak adhesion of IONPs on the ITO working electrode, resulting in poor stability and reproducibility. To overcome this issue, the self-assembly of the IONPs spontaneously on the disposable working electrode using functional groups is a good technique to form strong adhesion between the IONPs and the ITO electrode and improve the sensitivity due to their complexation with heavy metal ions. The functionalization of the ITO electrode using an amine-terminated silane self-assembly monolayer of 3-aminopropyltriethoxysilane (APTES) is favorable because of its simple process, high reproducibility, and good stability.<sup>22</sup> APTES consists of three hydrolysable ethoxy groups, leading to the formation of Si–O bonds, which is known as the silanization process, and an amine (NH<sub>2</sub>) from the aminopropyl groups points away from the surface allowing for electrostatic interactions with nanoparticles.<sup>23</sup> A better nanoparticle distribution on the ITO electrode can be achieved by APTES functionalization. Previously, nanoparticles like Au nanoparticles (AuNPs), reduced graphene oxide, and IONPs were self-assembled spontaneously on the disposable electrode (SPCE and ITO) using APTES for various types of electrochemical sensors.<sup>22,24,25</sup>

Khan et al.<sup>24</sup> reported the electrochemically reduced graphene oxide (ErGO) bound to the APTES-modified ITO electrode for the sensitive and selective electrochemical detection of tyramine. The strong binding between a negatively charged GO sheet with a positively charged NH<sub>2</sub> group on the ITO electrode through electrostatic interactions was formed. Ballarin et al.<sup>26</sup> fabricated the self-assembled monolayer of Au nanoparticles on the APTES-modified ITO electrode for electrochemical methanol detection. They reported that the NH<sub>2</sub> group from the APTES-ITO-modified electrode promoted high electron transfer and electrocatalytic activity. In our previous work, a bismuth nanosheet (BiNS) was used to modify an APTES-functionalized SPCE electrode (BiNS/APTES-SPCE) for Pb(II) and Cd(II) detection.<sup>27</sup> The APTES acted as a linker between the BiNS and SPCE electrode to form a strong bond and provide a large surface area for the

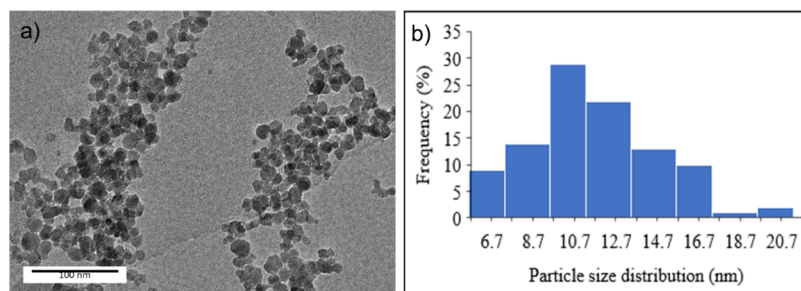


**Figure 1.** (a) TEM image of IONP-COOH and (b) particle size distribution of IONP-COOH.

uniform dispersion of BiNS on the SPCE electrode. However, the modified electrode (BiNS/APTES-SPCE) can only detect a single element at once.

In this work, IONP-COOH synthesized through coprecipitation were self-assembled on an APTES-ITO electrode for the simultaneous detection of heavy metal ions. The self-assembly process was achieved by electrostatic interactions between the negatively charged carboxyl ( $-\text{COOH}$ ) group that functionalized the IONPs and the positively charged amino ( $-\text{NH}_2$ ) group of the APTES-ITO modified electrode, thus forming covalent bonding. In this way, strong adhesion between the IONPs and the ITO electrode can be achieved, which then improves the electrochemical activity of the modified electrode. To the best of the authors' knowledge, the IONP-COOH/APTES-ITO-modified electrode as heavy metal sensors using an electrochemical technique has not been reported in literature so far. The effect of soaking time (30, 60, 90, and 120 min) of IONP-COOH self-assembled on an APTES-ITO electrode was studied in order to optimize the number of IONPs self-assembled on the APTES-ITO electrode, so that a larger electrochemical surface area of the modified electrode for heavy metal detection could be obtained. This is because a longer soaking time gives more time for the covalent bond in between IONP-COOH and  $-\text{NH}_2$  group of APTES to take place. The conductivity of the IONP-COOH/APTES-ITO-modified electrode and its ability to detect Cd(II) and Pb(II) ions simultaneously were investigated by using cyclic voltammetry (CV) and square wave anodic stripping voltammetry (SWASV) technique. Qualitative and quantitative measurements were conducted for the modified electrode IONP-COOH/APTE-ITO during electrochemical stripping analysis to investigate its sensitivity, selectivity, and applicability in a seawater sample for Cd(II)- and Pb(II)-ion detection.

## 2. RESULTS AND DISCUSSION

**2.1. Properties of IONPs.** The structure and morphology of synthesized IONP-COOH was observed using transmission electron microscopy (TEM) and X-ray diffraction (XRD) analysis. Figure 1a shows the TEM image of IONP-COOH, which was nearly spherical in shape. The particle size distribution of the synthesized IONP-COOH was measured for  $\sim 100$  particles (Figure 1b) by using ImageJ software. The mode particle size of the synthesized IONP-COOH was 10.7 nm.

Figure 2 shows the XRD pattern of the prepared IONP-COOH that corresponds to maghemite,  $\gamma\text{-Fe}_2\text{O}_3$  (JCPDS 039-1346). The diffraction peak showed the reflection planes indexed to (220), (311), (400), (422), (511), and (440) that correspond to peak position  $2\theta$  at 29.9, 35.4, 43.2, 53.6, 57.1,

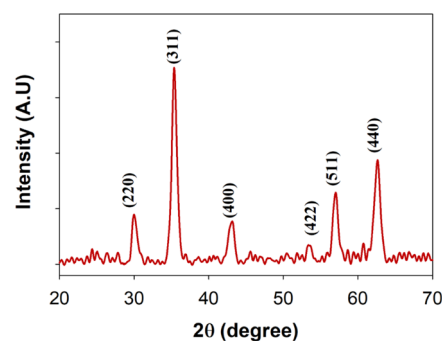


**Figure 2.** XRD pattern of IONP-COOH.

and  $62.7^\circ$ , respectively. The crystallite size calculated by using a Debye–Scherrer's equation<sup>9</sup> for the most intense peak (311) was about 12.8 nm, which is close to the value of the particle size of IONP-COOH measured from the TEM image ( $\sim 10.7$  nm).

**2.2. Properties of IONP-COOH/APTES-ITO Modified Electrode.** Figure 3 shows the FESEM images of bare ITO, IONP-COOH soaked without the APTES functionalization ITO electrode and IONP immobilized on the 5% APTES-functionalized ITO electrode with varying soaking times of 30, 60, 90, and 120 min (Figure 3c–f). Only a few IONP-COOH were observed on the ITO electrode without APTES functionalization (Figure 3b). This happens because only weak adhesion of IONP-COOH on the ITO electrode occurs in the absence of the amine functional group. Increasing the soaking time from 30 to 90 min increases the number of isolated IONP-COOH particles self-assembled on the APTES-ITO-modified electrode. A longer soaking time gives more time for covalent bond formation in between IONP-COOH and  $-\text{NH}_2$  groups of APTES to take place. However, at 90 min of soaking time, the isolated IONP-COOH aggregates assembled on the APTES-ITO was observed. At 120 min of soaking time, the agglomeration of IONP-COOH on the APTES-ITO-modified electrode was obvious. This observation showed that a soaking time of more than 90 min caused the agglomeration of IONPs deposited on the electrode surface. It is known that the IONP-COOH synthesized in this work is colloiddally stable with a negative charge, which was proven by the zeta potential analysis conducted for IONP-COOH at pH 7 with a value obtained being  $-52.7$  mV (Figure S1). Therefore, the agglomeration of IONP-COOH on the APTES-ITO-modified electrode may occur only if the interparticle repulsion between the negatively charged IONP-COOH is overcome. The reason for the agglomeration of IONP-COOH after a prolonged soaking time (120 min) is due to the protonated amino groups ( $\text{NH}_3^+$ ) that seem to exert their

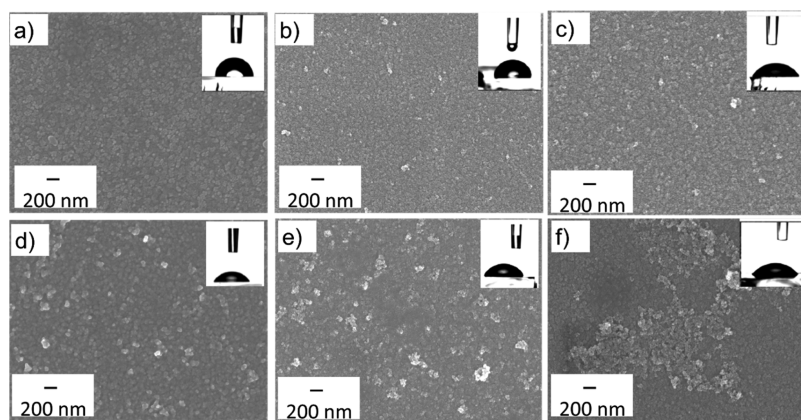


**Figure 3.** Distribution of IONPs on (a) bare ITO, (b) IONP-COOH/ITO, (c) 30 min soaked IONP-COOH/APTES-ITO, (d) 60 min soaked IONP-COOH/APTES-ITO, (e) 90 min soaked IONP-COOH/APTES-ITO, and (f) 120 min soaked IONP-COOH/APTES-ITO (inset: water contact angle).

attraction toward a larger number of IONP-COOH, resulting in the formation of small IONP-COOH aggregates.

After 90 min of soaking the IONP-COOH modified electrode, although agglomeration started to happen there were more IONP-COOH assembled on the APTES-ITO-modified electrode compared to 60 min of soaking in the IONP-COOH modified electrode. The IONP-COOH distribution for the 90 min soaked IONP-COOH-modified electrode was still well defined compared to the 120 min soaked IONP-COOH-modified electrode, where the agglomeration resulted in a lower surface area for the electrochemical reaction. A similar finding was also reported by Ballarin et al.,<sup>26</sup> where in their work the APTES-functionalized ITO electrode having a protonated  $\text{NH}_2$  group attracted toward a larger number of citrates charged AuNPs, thus resulting in the formation of small gold nanoparticle islands after a prolonged soaking time.

Water contact angle measurement was conducted to observe the effect of wettability on the APTES-functionalized ITO electrode and the effect of varying soaking times of IONP-COOH on the modification of the APTES-ITO modified electrode. The cross-sectional view of the water contact angles on the modified electrode is presented in the inset of Figure 3. The high wettability of the electrode (contact angle  $\leq 90^\circ$ ) encouraged the accessibility of the electrolyte toward the surface area of the electrode.<sup>28</sup> Figure 4 shows the comparison with bare ITO, the contact angle of the modified electrodes decreased with a prolonged soaking time of IONP-COOH, indicating an improvement in the wettability with an increase in a soaking time. The APTES-ITO had a lower water contact angle than bare ITO, implying that APTES provides wettability for the self-assembly of IONP-COOH on the electrode surface. Although the APTES concentration was fixed at 5%, the increase in the wettability of the electrodes was due to the carboxyl group of citric acid that was surface functionalized on the IONPs. This finding is supported by the contact angle measurement of IONP/ITO with respect to bare ITO; the average contact angle of IONP/ITO ( $85.06^\circ$ ) was lower than that of bare ITO ( $90.24^\circ$ ). Citric acid consists of three carboxyl groups in which a maximum of two carboxyl groups would bind to the nanoparticles leaving at least one carboxyl group free, thus eventually contributing to the hydrophilicity of the modified electrode.<sup>29</sup> Thus, 120 min of the IONP/APTES-ITO electrode has the highest surface wettability (contact

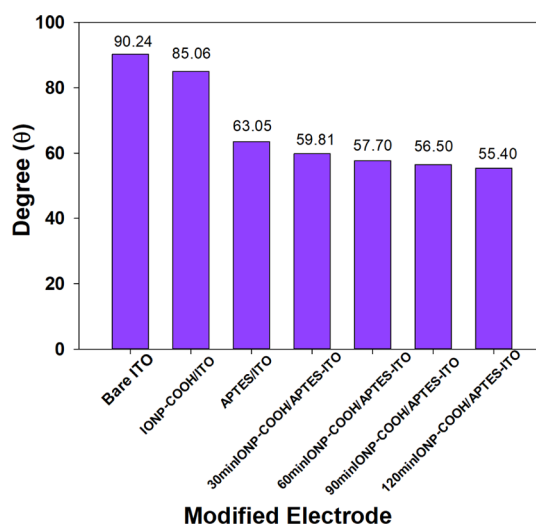


**Figure 4.** Water contact angle measurement of the modified electrode.

angle:  $44.79^\circ$ ) because many IONPs that were surface functionalized with citric acid had self-assembled on the APTES-functionalized ITO electrode.

APTES is commonly applied to prepare an amine-functionalized self-assembled monolayer on the ITO electrode, which will have high affinity for the attachment of nanoparticles. APTES consists of three hydrolysable ethoxy ( $-\text{O}-\text{CH}_2-\text{CH}_3$ ) groups and amine groups ( $\text{NH}_2$ ) at its terminal.<sup>30</sup> Figure 5 illustrates the functionalization of the APTES-ITO electrode and modification of IONP-COOH on the APTES-ITO. After the ITO electrode was cleaned with the RCA method, a hydroxyl group formed on its surface. When the ITO electrode was soaked in a 5% APTES solution, silanols ( $\text{Si}-\text{O}-\text{H}$ ) were generated from the hydrolysis of the ethoxy group in APTES (Figure 5a). These silanols then condensed with the hydroxyl group formed on the surface of the ITO electrode, thus forming a monolayer of APTES molecules through covalent bonding. In such configurations, a higher availability of the amine group pointing away from the ITO electrode allows further functionalization with nanoparticles. After the functionalization of APTES on the ITO electrode, the electrode was soaked in 2 mg/mL IONP-COOH solution (Figure 5b). The amine group ( $-\text{NH}_2$ ) is protonated at

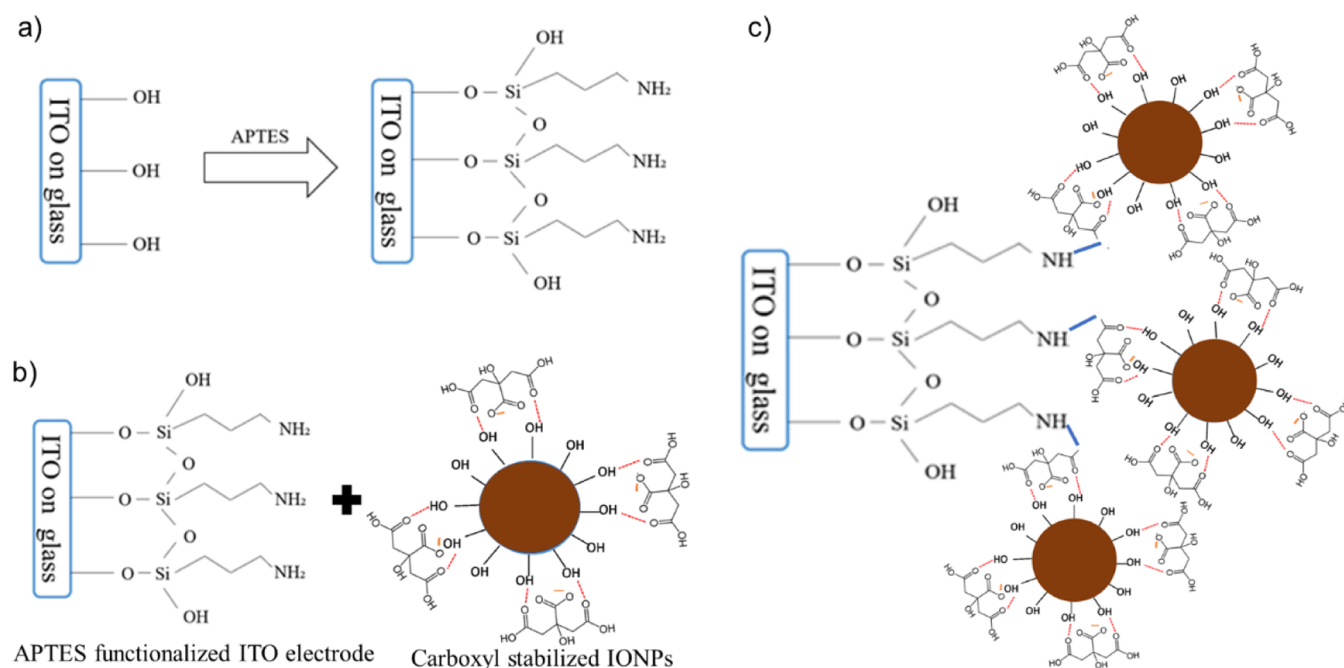


**Figure 5.** Schematic illustration of (a) APTES functionalization on ITO, (b) APTES-functionalized ITO electrode and carboxyl-stabilized IONPs, and (c) self-assembly of IONPs-COOH on the APTES-ITO electrode.

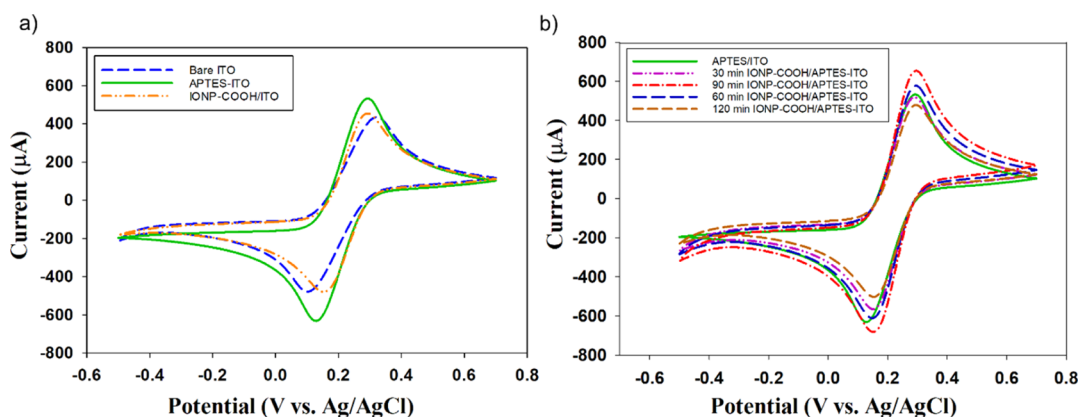


**Figure 6.** CV analysis of (a) bare ITO, APTES-ITO, and IONP-COOH/ITO and (b) APTES-ITO-modified electrode with varied soaking times of IONP-COOH in 5 mM of  $K_3Fe(CN)_6$  containing 0.1 M KCl at 50 mV/s scan rate.

**Table 1.** Summary of the Electrochemical Performance of the Modified Electrode

electrode	$I_{pa}$ ( $\mu A$ )	$I_{pc}$ (V)	$E_{pa}$ (V)	$E_{pc}$ (V)	$\Delta E_p$ (V)	slope $I_{pa}$ vs $v^{1/2}$	effective surface area, $A_e$ ( $cm^2$ )
bare ITO	527.98	-478.50	0.32	0.10	0.22	$2.02 \times 10^{-3}$	0.581
APTES-ITO	587.34	-631.08	0.29	0.13	0.16	$2.48 \times 10^{-3}$	0.711
30 min IONP-COOH/APTES-ITO	598.62	-530.38	0.29	0.16	0.13	$2.65 \times 10^{-3}$	0.761
60 min IONP-COOH/APTES-ITO	681.06	-611.92	0.29	0.15	0.14	$3.05 \times 10^{-3}$	0.876
90 min IONP-COOH/APTES-ITO	770.02	-682.70	0.30	0.15	0.15	$3.33 \times 10^{-3}$	0.957
120 min IONP-COOH/APTES-ITO	566.60	-502.80	0.30	0.15	0.15	$2.45 \times 10^{-3}$	0.704
IONPs/ITO	545.69	-479.90	0.29	0.15	0.14	$2.37 \times 10^{-3}$	0.681

neutral pH. As a result, the IONP-COOH with a negatively charged carboxyl group ( $-COOH$ ) electrostatically attracted toward positively charged amine at the end of the APTES-ITO modified electrode to form covalent bonding. Thus, a self-assembled monolayer of IONP-COOH was formed on the APTES-functionalized ITO electrode (Figure 5c).

The electrochemical characterization for the effect of soaking time for IONP-COOH (30, 60, 90, and 120 min)

on the APTES-ITO-modified electrode was studied using CV analysis. Figure 6 shows the CV graph and Table 1 lists the summary of the electrochemical performance for the bare ITO electrode, APTES-ITO, IONP-COOH/ITO, 30 min IONP-COOH/APTES-ITO, 60 min IONP-COOH/APTES-ITO, 90 min IONP-COOH/APTES-ITO, and 120 min IONP-COOH/APTES-ITO in the electrolyte of 5 mM  $K_4Fe(CN)_6$  containing 0.1 M KCl solution. Figure 6a shows a low anodic

peak current ( $I_{pa}$ ) of 527.98  $\mu\text{A}$  and large peak to peak potential difference ( $\Delta E_p$ ) of 0.22 V for the bare ITO electrode. After modification of ITO with APTES, the  $I_{pa}$  value increases to 587.34  $\mu\text{A}$  and  $\Delta E_p$  reduces to 0.16 V, which indicate increasing concentration and ease of electronic transport of the  $[\text{Fe}(\text{CN})_6^{3-/4-}]$  anionic probes due to its strong affinity toward the polycationic layer as the amino groups of the APTES get protonated ( $\text{NH}_3^+$ ) in aqueous solution.<sup>26</sup> The IONP-COOH/ITO-modified electrode without APTES modification shows an increment in  $I_{pa}$  (545.69  $\mu\text{A}$ ) and lower in  $\Delta E_p$  (0.14 V) compared to the bare ITO electrode. The improvement in the peak current value is because of the IONP-COOH increases the electrochemical surface area and facilitates the electron transfer for the  $[\text{Fe}(\text{CN})_6^{3-/4-}]$  redox reaction.<sup>9</sup>

After modification of the APTES-ITO electrode with a self-assembly of IONP-COOH, the current response increases with a prolonged soaking time of IONP-COOH from 30 to 90 min, indicating an improvement in the electrochemical active surface area of the modified electrode compared with that of the bare ITO electrode, APTES-ITO, and IONP-COOH/ITO-modified electrode. 90 min IONP-COOH/APTES-ITO-modified electrode shows the highest  $I_{pa}$  value (770.02  $\mu\text{A}$ ) due to a longer time for IONP-COOH self-assembled on the APTES-ITO, and thus provided an additional electrochemical surface area. This phenomenon intensified the redox reaction on the electrode/solution interface, thus increasing the current response of the electrode from 30 to 90 min soaking time in IONP-COOH. However, when the soaking time was further increased to 120 min, the peak current value dropped (566.60  $\mu\text{A}$ ). This finding could be attributed to the lesser surface area available for the  $[\text{Fe}(\text{CN})_6^{3-/4-}]$  redox reaction. After 120 min of soaking time, a larger number of IONP-COOH was attracted toward protonated amino groups ( $\text{NH}_3^+$ ) of the APTES-functionalized ITO electrode, thereby causing the agglomeration of the IONP-COOH and reducing the active surface area available for the redox reaction, as can be seen in Figure 3.

The effective surface area  $A_e$  of the modified electrode was calculated by using the Randles–Sevcik equation,<sup>31,32</sup> and the values are tabulated in Table 1. The detailed calculation of  $A_e$  is discussed in the Supplementary Information (Figure S2). The  $A_e$  of the modified electrode increased when the  $I_p$  increased from 30 to 90 min soaking time in IONP-COOH in a 5% APTES-functionalized ITO electrode. This result is due to the increase in IONP-COOH deposited on the APTES-functionalized electrode as supported by the FESEM images in Figure 3c–f for 30–90 min of soaking time. The  $A_e$  started to decrease for an IONP-COOH soaking time of 120 min because of the highly agglomerated IONP-COOH deposited on the electrode surface, as shown in the FESEM images in Figure 3f. This finding revealed that the 90 min IONP-COOH/APTES-ITO modified electrode has the highest active surface area for electron transfer and presence of less agglomerated IONP-COOH (Figure 3f). For further investigation on Cd(II) and Pb(II) detection, the 90 min IONP-COOH/APTES-ITO was chosen.

**2.3. Simultaneous Determination of Cd(II) and Pb(II) Ions.** As shown in Figure 7, SWASV analysis was conducted on the bare ITO, APTES-ITO, IONP-COOH/ITO, and 90 min IONP-COOH/APTES-ITO electrodes for the simultaneous detection of 100 ppb Cd(II) and Pb(II) ions in 0.1 M acetate buffer. For the bare ITO electrode, no distinct stripping

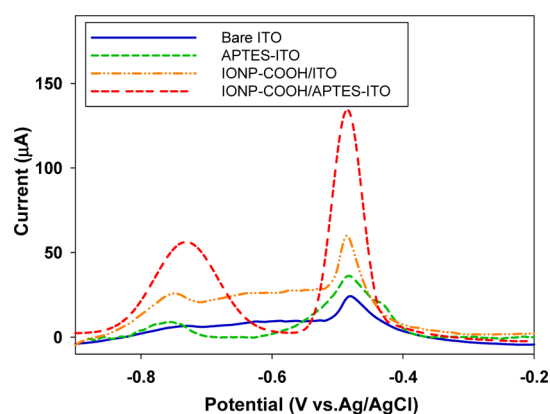


**Figure 7.** SWASV analysis curves of different modified electrodes in the presence of 100 ppb Cd(II) and Pb(II) ions in 0.1 M acetate buffer solution (pH 4.5) with a deposition potential of  $-1.0$  V and deposition time of 180 s.

peak was observed for Cd(II) ions, and only a small stripping peak at  $-0.48$  V (13.94  $\mu\text{A}$ ) was observed for Pb(II) ions. The APTES-ITO-modified electrode showed a low stripping current value for Pb(II) and improved Cd(II) current values at  $-0.75$  and  $-0.48$  V (9.59 and 28.1  $\mu\text{A}$ ), respectively. The presence of the amino group of APTES increases the adsorption ability of the APTES-ITO-modified electrode toward heavy metal ions. The IONP-COOH/ITO-modified electrode showed two distinct peaks and improved stripping current value at  $-0.75$  and  $-0.48$  V (17.16 and 37.2  $\mu\text{A}$ ) for the simultaneous detection of Cd(II) and Pb(II) ions. The 90 min IONP-COOH/APTES-ITO-modified electrode showed well-defined Cd(II) and Pb(II) ions at  $-0.75$  and  $-0.48$  V with higher peak current values of 54.3 and 125.2  $\mu\text{A}$ , respectively. The possible reasons for the distinct peaks and improved stripping peak current of Cd(II) and Pb(II) with the presence of IONP-COOH on the ITO electrode are the high absorption ability of IONPs toward heavy metal ions, the large surface area provided by IONPs for the deposition of heavy metal ions, the presence of negatively charged COOH that provides strong affinity toward positively charged heavy metal ions to be attracted and deposited, and the ability of IONPs to actively participate in reducing heavy metal ions to its zero oxidation state during preconcentration. As for the IONP-COOH/APTES-ITO-modified electrode, the enhancement in the stripping peak was observed. The reasons are that more IONP-COOH self-assembled on the APTES-ITO-modified electrode and the high affinity of the amino groups from APTES to adsorb and form complexation with heavy metal ions. The complexation occurred due to the acid–base pairing interaction between the electron-rich amino ligands and electron-deficient heavy metal ions. A similar mechanism was also reported by other researchers on the ability of amino group to increase heavy metal ion absorption.<sup>21</sup>

The optimization of operational parameters, such as the deposition potential and deposition time, was conducted to obtain high sensitivity and good reproducibility of the modified electrode for the simultaneous Cd(II) and Pb(II) detection using the SWASV technique. The effect of the deposition potential was observed from  $-1.4$  to  $-0.8$  V for the simultaneous detection of 100 ppb Cd(II) and Pb(II) in 0.1 M acetate buffer solution (pH 4.5). As shown in Figure S3, stripping peak current values increase with a potential increased from  $-0.8$  to  $-1.0$  V. At a more negative potential

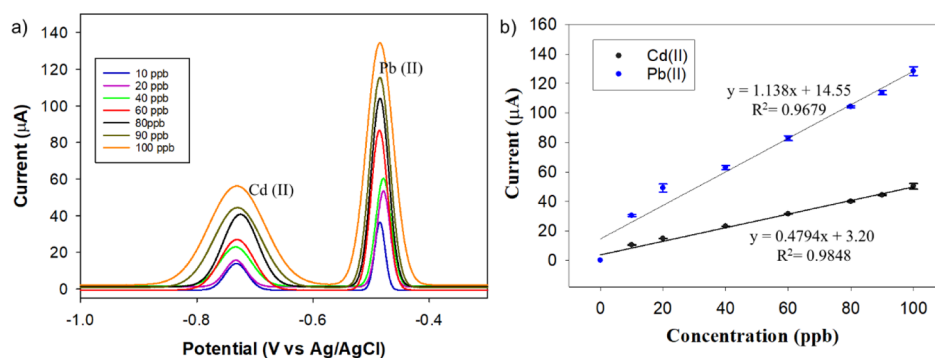


**Figure 8.** (a) SWASV curves of the 90 min IONP-COOH/APTES-ITO-modified electrode stripping peak of Cd(II) and Pb(II) simultaneous detection for 10 to 100 ppb, and (b) linear calibration plot for Cd(II) and Pb(II) with concentrations ranging from 10 to 100 ppb in 0.1 M acetate buffer solution (pH 4.5) with a deposition potential of  $-1.0$  V and deposition time of 180 s ( $n = 3$ ).

**Table 2.** Comparison of Previous Works and the Present Work for Simultaneous Cd(II) and Pb(II) Ion Detection

modified electrode	linear range (ppb)		LOD (ppb)		references
	Cd(II)	Pb(II)	Cd(II)	Pb(II)	
nanoplate-stacked $\text{Fe}_3\text{O}_4/\text{GCE}$	11.2–224.8	20.8–373	23.94	12.34	33
$\text{Fe}_3\text{O}_4$ NP-chitosan/GCE	134.9–191.1	20.7–269.4	4.41	8.74	34
$\text{Fe}_3\text{O}_4/\text{F-MWCNT}/\text{GCE}$	56.2–3372	103.6–6216	5.62	16.58	14
$\text{Fe}_3\text{O}_4@\text{G}_2\text{-PAD}/\text{MCPE}$	0.5–80	0.5–80	0.21	0.17	13
Fe-Al-CS/GCE	0.005–0.125	0.005–0.125	0.07	0.03	21
IONP-COOH/APTES-ITO	10–100	10–100	0.90	0.60	this work

lower than  $-1.0$  V, the stripping peak current value starts to reduce. This happens because  $\text{H}_2$  evolution starts forming near the electrode surface, which deteriorates the modified electrode surface and causes modified layer to peel off. Therefore, the optimum deposition potential for the simultaneous detection of 100 ppb Cd(II) and Pb(II) using an IONP-COOH/APTES-ITO-modified electrode is at  $-1.0$  V.

The deposition time was varied from 120 to 240 s for the simultaneous detection of 100 ppb Cd(II) and Pb(II) in 0.1 M acetate buffer solution (pH 4.5). Increases in the deposition time from 120 to 180 s increases the stripping peak current value. This happens because more heavy metal ions are deposited at a longer deposition time. However, further increase in the deposition time to 200 and 240 s, showed no remarkable improvement. The reason is because the modified electrode surface area has achieved saturation. Therefore, the optimum deposition time for the simultaneous detection of 100 ppb Cd(II) and Pb(II) using the IONP-COOH/APTES-ITO-modified electrode is at 180 s.

The applicability of the 90 min IONP-COOH/APTES-ITO-modified electrode was then subjected to SWASV analysis for the simultaneous detection of the Cd(II)- and Pb(II)-ion mixture with varying concentrations (10–100 ppb) to determine its linearity and LOD. As shown in Figure 8a, the two distinctive stripping peaks of Cd(II) and Pb(II) increased linearly with the concentration of ion mixtures from 10 to 100 ppb at  $-0.75$  and  $-0.48$  V, respectively. Figure 8b shows the linear calibration plot represented as  $I_{p,\text{Cd}} (\mu\text{A}) = 0.45C + 5.09$  with a correlation coefficient  $R^2$  of 0.9876 for Cd(II) ions and  $I_{p,\text{Pb}} (\mu\text{A}) = 0.99C + 25.93$  with a correlation coefficient  $R^2$  of 0.996 for Pb(II) ions.

Comparison of the linear range and LOD was conducted for the IONP-COOH-modified electrode in the present work and previous studies for the simultaneous detection of Cd(II) and

Pb(II). The results in Table 2 show that the IONP-COOH/APTES-ITO-modified electrode from the present work has comparable LOD and wider linearity compared with the  $\text{Fe}_3\text{O}_4@\text{G}_2\text{-PAD}/\text{MCPE}$ ,<sup>13</sup> nanoplate-stacked  $\text{Fe}_3\text{O}_4/\text{GCE}$ ,<sup>33</sup> and  $\text{Fe}_3\text{O}_4$ -chitosan/GCE.<sup>34</sup> The LODs obtained from the linear calibration plot for the simultaneous detection of Cd(II) and Pb(II) are 0.90 and 0.60 ppb, respectively. These results were obtained because the stripping current peak value for Cd(II) and Pb(II) is high even at low concentrations of Cd and Pb ions.

In addition, the fabrication technique for IONP-COOH on the electrode surface in this work is different from previous studies. All previous works mentioned in Table 2 reported the modification of the electrode with iron oxide nanoparticles using a drop-casting method. In the present work, the IONPs was self-assembled on the surface of the ITO electrode with the aid of an APTES linker. This self-assembly led to the good adhesion of IONPs on the surface of the ITO electrode, thus increasing the electrochemical active surface area of IONPs for the accumulation of Cd(II) and Pb(II) on the electrode surface. Hence, a low LOD was achieved. Another possible reason for the low LOD in the simultaneous detection of Cd(II) and Pb(II) is the improved chemical binding between the  $-\text{COOH}$  group of IONPs and the amine group of APTES-ITO. Some of the modified electrodes showed a lower LOD than that reported in the present work.<sup>14,21</sup> The hybrid combination of nanomaterials or nanocomposites has improved the conductivity and active surface area for the simultaneous heavy metal detection. However, these electrodes may require an additional process for nanoparticle synthesis, thus increasing the complexity of the modification technique and the cost of the modified electrode.

**2.4. Interference, Repeatability, and Reproducibility Study.** The interference study was performed to determine the selectivity of the IONP-COOH/APTES-ITO-modified elec-

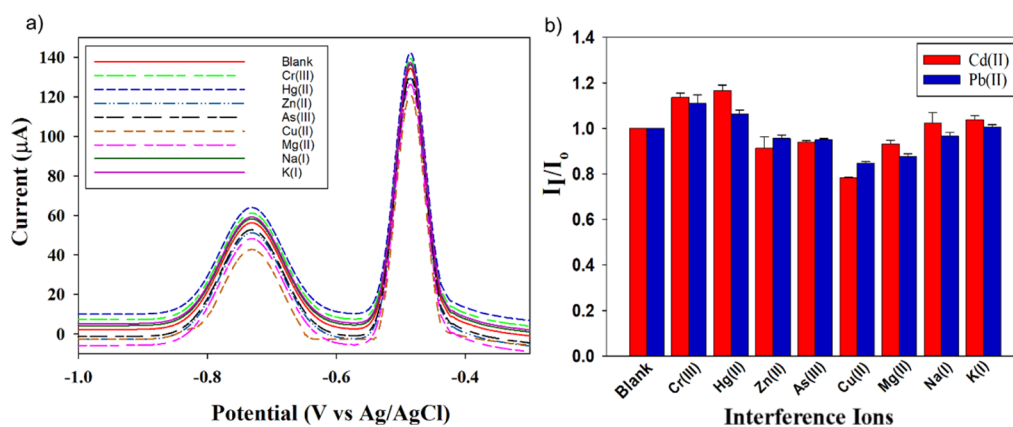


**Figure 9.** (a) SWASV response and (b) interference response current ratio ( $I_1/I_0$ ) of the IONP-COOH/APTES-ITO-modified electrode in 100 ppb Cd(II) and Pb(II) standard solution contain 100 ppb interference ions of the Cr(III), Hg(II), Zn(II), Cu(II), Mg(II), Na(I), and K(I) standard solution ( $n = 3$ ).

**Table 3.** Comparison on the Determination of Cd(II) and Pb(II) in the Seawater Samples Using SWASV Analysis of the Modified Electrode and ICP-OES Spectroscopy Technique

sample	spiked (ppb)		SWASV analysis using a modified electrode (ppb)		recovery (ppb)		ICP-OES analysis (ppb)	
	Cd(II)	Pb(II)	Cd(II)	Pb(II)	Cd(II)	Pb(II)	Cd(II)	Pb(II)
Malacca Street A			1.77	2.68			ND	ND
	10	10	12.10	12.89	103.32	103.18	11.65	9.72
	30	30	32.53	32.54	102.53	99.54	31.99	26.54
	50	50	53.55	54.06	103.56	102.76	51.15	50.85
Malacca Street B				3.54			ND	ND

trode toward the simultaneous detection of Cd(II) and Pb(II). In this analysis, the SWASV peak response of the IONP-COOH/APTES-ITO-modified electrode in the simultaneous detection of 100 ppb Cd(II) and Pb(II) standard solution were compared with a SWASV peak response with the addition of 100 ppb single element interference ions of Cr(III), Hg(II), Zn(II), Cu(II), Mg(II), Na(I), and K(I) and the multielement interference ions containing 23 metal ions [Ag(I), Al(III), B(II), Ba(II), Bi(III), Ca(II), Cd(II), Co(II), Cr(III), Fe(II), Ga(III), In(III), K(I), Li(I), Mg(II), Mn(II), Na(I), Ni(II), Pb(II), Sr(II), Tl(I), Hg(II) and Zn(II)] in a 0.1 M acetate buffer solution.

Figure 9 shows the SWASV peak response, and the peak of the current ratio with the presence of interference ions ( $I_1$ ) over without the presence of interference ions ( $I_0$ ) for the IONP-COOH/APTES-ITO-modified electrode. The value of  $I_1/I_0$  close to 1 indicate a high anti-interference ability. These findings showed little changes in Cd(II) and Pb(II) peak currents when the Cr(III), Hg(II), Zn(II), As(III), Mg(II), Na(I), and K(I) interference ion presence. However, peak currents of Cd(II) and Pb(II) further dropped when the Cu(II) interference ions were added due to the formation of Pb–Cu and Cd–Cu intermetallic compound during anodic stripping, which is in agreement with other reported works.<sup>35–37</sup>

The selectivity for the IONP-COOH/APTES-ITO-modified electrode was also tested in the ICP multielement standard solution (containing 23 multielement). As shown in Figure S5, after the addition of 5 ppb multielement standard solution into 100 ppb Cd(II) and Pb(II) standard solution, only slight decreased in the peak currents of Cd(II) and Pb(II). However, the peak current values for Cd(II) and Pb(II) were suppressed

to the ratios of 0.48 and 0.5, respectively, if analyzed in 100 ppb multielement standard solution. This finding shows that at high concentrations (100 ppb) of 23 types the heavy metal ion mixture may interfere in the oxidation and reduction of Cd/Cd(II) and Pb/Pb(II). The competition for adsorptive sites between Cd(II) and Pb(II) ions and other coexisting metal ions, formation of intermetallic compounds, and variation of ion diffusion coefficient resulted in the peak current value decrease. The peak potential for Cd(II) and Pb(II) remained unchanged in the presence of Cr(III), Hg(II), Zn(II), and Cu(II) interference ion which indicated that the IONP-COOH/APTES-ITO-modified electrodes showed good selectivity toward the simultaneous detection of Cd(II) and Pb(II).

There was a ~20 mV peak potential shift toward the negative for Cd(II) and Pb(II) in a 100 ppb multielement solution due to the decrease in the amount of Cd(II) and Pb(II) deposited and stripped off. Theoretically, peak potential shifts in SWASV are mainly influenced by the morphology, orientation, and compacity of the heavy metal ions deposited on the working electrode during preconcentration, thus leading to variation in kinetics and thermodynamics during the stripping process.<sup>37</sup> The reproducibility of five IONP-COOH/APTES-ITO-modified electrodes was examined for the simultaneous detection of 100 ppb Cd(II) and Pb(II) ions using a SWASV technique yielding a relative standard deviations of 4.02 and 4.56% (Figure S5), respectively.

**2.5. Application in Seawater Sample.** Seawater samples were collected and used to observe the practical applicability of the IONP-COOH/APTES-ITO-modified electrode in detecting Cd(II) and Pb(II) ions with SWASV. The concentrations of Cd(II) and Pb(II) ions in the seawater sample taken at Malacca Street A were 1.77 and 2.68 ppb, respectively. As for

Malacca Street B, only Pb(II) ions were detected with a concentration of 3.54 ppb. The applicability of the IONP-COOH/APTES-ITO-modified electrode was evaluated with recovery evolution using the standard addition method of Cd(II) and Pb(II) standard solutions. The seawater samples with similar conditions were spiked with mixed Cd(II) and Pb(II) ion standard solutions at 10, 30, and 50 ppb. Good recoveries were obtained, as shown in Table 3. SWASV analysis results were compared with the ICP-OES spectroscopy results for the seawater sample to confirm the applicability of the IONP-COOH/APTES-ITO-modified electrode in an actual sample measurement. The results showed that the IONP-COOH/APTES-ITO-modified electrode has a great application potential in the electrochemical heavy metal detection for real samples.

### 3. CONCLUSIONS

IONPs with a maghemite phase ( $\gamma\text{-Fe}_2\text{O}_3$ ) were synthesized through co-precipitation. The as-synthesized IONP-COOH was self-assembled on the APTES-functionalized ITO electrode. The effect of the IONP-COOH soaking time on the APTES-ITO electrode was investigated. A 90 min soaking time for IONP-COOH/APTES-ITO produced high conductivity and effective surface area  $A_e$  and thus was chosen for further investigation on heavy metal detection by the SWASV technique. The IONP-COOH-modified electrodes are sensitive toward the simultaneous detection of Cd(II) and Pb(II) within a linear range of 10–100 ppb and LODs of 0.903 and 0.597 ppb, respectively. The IONP-COOH/APTES-ITO-modified electrode is highly sensitive and showed good selectivity for Cd(II) and Pb(II) simultaneous detection. Finally, the IONP-COOH/APTES-ITO-modified electrode was applied for seawater samples. Cd(II) was detected with concentrations of 2.68 and 3.54 ppb in the samples taken from two places along the Malacca street area.

### 4. EXPERIMENTAL PROCEDURE

**4.1. Preparation of IONPs.** IONPs were synthesized through co-precipitation under a  $\text{N}_2$  gas atmosphere.  $\text{FeCl}_2$  and  $\text{FeCl}_3$  solutions in the ratio of 1:2 M was slowly poured into a reactor containing 500 mL of NaCl and stirred at 500 rpm for approximately 10–15 min. The pH of the solution was controlled at 10 throughout the reaction by dropwise adding NaOH.  $\text{N}_2$  flow was stopped after 15 min, and the solution was left to stand for 2 h. The supernatant was then removed, and the precipitate of IONPs was washed with distilled water and collected for functionalization. IONP precipitates were stabilized using citric acid at post-synthesis under room temperature.<sup>38</sup> The IONP-COOH particles were then collected, washed with distilled water, and dispersed into 50 mL of distilled water. X-ray diffraction (XRD) was applied to identify the phase of IONPs, and transmission electron microscopy (TEM) was used to determine the particle size of IONPs.

**4.2. Preparation of IONP-Modified Electrode.** The ITO glass electrode was cleaned using the Radio Corporation of America (RCA) method,<sup>38</sup> soaked in ethanol containing 5 wt % APTES solution for 2 h, and finally rinsed with ethanol and oven dried at 80 °C. IONP-COOH was self-assembled on the APTES-functionalized ITO electrodes by immersing the APTES-ITO electrode later in 2 mg/mL IONP-COOH solution at varying soaking times (30, 60, 90, and 120 min).

The modified IONP-COOH/APTES-ITO glass was rinsed with distilled water to remove unbound IONP-COOH on the APTES-ITO and dried at room temperature. The water contact angle of the modified electrode was measured using a contact angle goniometer (KSV CAM 101) to observe the effect of the wettability of the APTES-functionalized ITO electrode and varying soaking times for IONP-COOH on the modification of the APTES-ITO electrode. Millipore water was gently dropped onto the sample surface using a syringe. All measurements were performed for 30 s after the water droplet was positioned to obtain a stable contact angle.

**4.3. Electrochemical Measurements by Using CV and SWASV.** The electrochemical measurement of CV and SWASV were performed using a DropSens- $\mu\text{Stat}$  400 Bipotentiostat/Galvanostat (DropSens, Spain) based on a three-electrode cell. A platinum rod represents the counter electrode, Ag/AgCl (3 M KCl) as the reference electrode, and a bare ITO electrode and IONP-COOH/APTES-ITO-modified electrode as the working electrode. CV analysis was conducted at a potential scan range from  $-0.5$  to  $0.7$  V, scan rate  $50$  mV/s in  $5.0$  mM potassium ferricyanide(III),  $[\text{Fe}(\text{CN})_6]^{3-/4-}$  with the presence of  $0.1$  M potassium chloride (KCl) solution as the supporting electrolyte. The electrochemical characterization of the modified electrodes of IONP-COOH at varying soaking times (30, 60, 90, and 120 min) on the APTES-ITO electrode was measured using CV.

The SWASV technique was performed for simultaneously detect Cd(II) and Pb(II) ions in  $0.1$  M acetate buffer solution (pH 4.5) under continuous stirring. The analysis was performed to determine the linear range and LOD of the IONP-COOH/APTES-ITO-modified electrode toward Cd(II) and Pb(II) under deposition potential  $-1.0$  V (vs Ag/AgCl), deposition time of 180 s, amplitude of  $0.05$  V, frequency of  $25$  Hz, step potential of  $0.005$  V, and potential scan range from  $-0.9$  to  $-0.3$  V.

**4.4. Interference Study.** Interference measurement was performed to determine the selectivity and possible interference of the IONP-COOH/APTES-ITO-modified electrode for the simultaneous detection of Cd(II) and Pb(II) ions. The measurement was analyzed using SWASV analysis in  $0.1$  M acetate buffer solution (pH 4.5) containing  $100$  ppb Cd(II) and Pb(II) ions and addition of  $100$  ppb possible interference ions of Cr(III), Hg(II), Zn(II), Cu(II), Mg(II), Na(I), K(I), and ICP-multi element standard stock solution (111355 Supelco). The ICP-multielement solution contains 23 different types of metal ions of Ag(I), Al(III), B(II), Ba(II), Bi(III), Ca(II), Cd(II), Co(II), Cr(III), Fe(II), Ga(III), In(III), K(I), Li(I), Mg(II), Mn(II), Na(I), Ni(II), Pb(II), Sr(II), Tl(I), Hg(II), and Zn(II).

**4.5. Application in Seawater Sample.** Real sample analysis and validation were conducted to observe the applicability of the IONP-COOH/APTES-ITO-modified electrode. Seawater samples were collected in two spots along Malacca street on 13 August 2020 at 10.00 am, filtered using  $0.25$   $\mu\text{m}$  filter paper, and diluted with  $0.1$  M acetate buffer (pH 4.5) with a volume ratio of 1:5. SWASV technique was used to evaluate the Cd(II) and Pb(II) ion concentration in the seawater samples before and after being spiked with known concentrations of 10, 30, and 50 ppb mixture of Cd(II) and Pb(II) ions. The obtained results were compared with those from seawater measured using ICP-OES spectroscopy.

## ■ ASSOCIATED CONTENT

### SI Supporting Information

The Supporting Information is available free of charge at <https://pubs.acs.org/doi/10.1021/acsomega.1c07158>.

Zeta potential result of IONP-COOH; CV with varying scan rates of 10, 20, 30, 40, and 50 mV/s for the bare ITO and modified electrode with varying IONP-COOH soaking times; SWASV analysis of the 90 min IONP-COOH/APTES-ITO modified electrode with optimization parameters; reproducibility of 90 min IONP-COOH/APTES-ITO-modified electrode for simultaneous detection of 100 ppb Cd(II) and Pb(II) ions; interference response current ratio ( $I_1/I_0$ ) of IONP-COOH/APTES-ITO-modified electrode in 100 ppb Cd(II) and Pb(II) standard solutions, and in 23 multielement standard solution (PDF)

## ■ AUTHOR INFORMATION

### Corresponding Author

**Khairunisak Abdul Razak** – School of Materials & Mineral Resources Engineering, Universiti Sains Malaysia, 14300 Nibong Tebal, Pulau Pinang, Malaysia; NanoBiotechnology Research and Innovation (NanoBRI), Institute for Research in Molecular Medicine, Universiti Sains Malaysia, 11800 Penang, Malaysia; [orcid.org/0000-0003-0140-2418](https://orcid.org/0000-0003-0140-2418); Email: [khairunisak@usm.my](mailto:khairunisak@usm.my)

### Authors

**Noorhashimah Mohamad Nor** – School of Materials & Mineral Resources Engineering, Universiti Sains Malaysia, 14300 Nibong Tebal, Pulau Pinang, Malaysia; [orcid.org/0000-0001-5692-8287](https://orcid.org/0000-0001-5692-8287)

**Sarasijah Arivalakan** – School of Materials & Mineral Resources Engineering, Universiti Sains Malaysia, 14300 Nibong Tebal, Pulau Pinang, Malaysia

**Nor Dyana Zakaria** – NanoBiotechnology Research and Innovation (NanoBRI), Institute for Research in Molecular Medicine, Universiti Sains Malaysia, 11800 Penang, Malaysia

**Nithiyaa Nilamani** – Centre for Marine and Coastal Studies, Universiti Sains Malaysia, 11800 Penang, Malaysia

**Zainovia Lockman** – School of Materials & Mineral Resources Engineering, Universiti Sains Malaysia, 14300 Nibong Tebal, Pulau Pinang, Malaysia; [orcid.org/0000-0002-1535-8035](https://orcid.org/0000-0002-1535-8035)

Complete contact information is available at: <https://pubs.acs.org/doi/10.1021/acsomega.1c07158>

### Notes

The authors declare no competing financial interest.

## ■ ACKNOWLEDGMENTS

This project was funded by Research University grant 1001/Pbahan/8700049 and FRGS 304/PBahan/6071464. The authors gratefully acknowledge the support from the technical staff from School of Materials and Mineral Resources Engineering, and INFORMM. The authors acknowledge sample collection by Centre for Marine and Coastal Studies (CEMACS), Universiti Sains Malaysia.

## ■ REFERENCES

- (1) Srivastava, N. K.; Majumder, C. B. Novel biofiltration methods for the treatment of heavy metals from industrial wastewater. *J. Hazard. Mater.* **2008**, *151*, 1–8.
- (2) Tytla, M. Assessment of Heavy Metal Pollution and Potential Ecological Risk in Sewage Sludge from Municipal Wastewater Treatment Plant Located in the Most Industrialized Region in Poland-Case Study. *Int. J. Environ. Res. Public Health* **2019**, *16*, 2430.
- (3) Buledi, J. A.; Amin, S.; Haider, S. I.; Bhangar, M. I.; Solangi, A. R. A review on detection of heavy metals from aqueous media using nanomaterial-based sensors. *Environ. Sci. Pollut. Res.* **2020**, *28*, 58994–59002.
- (4) Ji, W. B.; Yap, S. H. K.; Panwar, N.; Zhang, L. L.; Lin, B.; Yong, K. T.; Tjin, S. C.; Ng, W. J.; Majid, M. B. A. Detection of low-concentration heavy metal ions using optical microfiber sensor. *Sens. Actuators, B* **2016**, *237*, 142–149.
- (5) Hou, H.; Zeinu, K. M.; Gao, S.; Liu, B.; Yang, J.; Hu, J. Recent Advances and Perspective on Design and Synthesis of Electrode Materials for Electrochemical Sensing of Heavy Metals. *Energy Environ. Mater.* **2018**, *1*, 113–131.
- (6) Lu, Z.; Zhang, J.; Dai, W.; Lin, X.; Ye, J.; Ye, J. A screen-printed carbon electrode modified with a bismuth film and gold nanoparticles for simultaneous stripping voltammetric determination of Zn(II), Pb(II) and Cu(II). *Microchim. Acta* **2017**, *184*, 4731–4740.
- (7) Palisoc, S. T.; Natividad, M. T.; De Jesus, N.; Carlos, J. Highly Sensitive AgNP/MWCNT/Nafion Modified GCE-Based Sensor for the Determination of Heavy Metals in Organic and Non-organic Vegetables. *Sci. Rep.* **2018**, *8*, 17445.
- (8) Zhao, G.; Wang, H.; Liu, G. Sensitive determination of trace Cd(II) and Pb(II) in soil by an improved stripping voltammetry method using two different in situ plated bismuth-film electrodes based on a novel electrochemical measurement system. *RSC Adv.* **2018**, *8*, 5079–5089.
- (9) Deshmukh, S.; Kandasamy, G.; Upadhyay, R. K.; Bhattacharya, G.; Banerjee, D.; Maity, D.; Deshusses, M. A.; Roy, S. S. Terephthalic acid capped iron oxide nanoparticles for sensitive electrochemical detection of heavy metal ions in water. *J. Electroanal. Chem.* **2017**, *788*, 91–98.
- (10) Gounden, D.; Khene, S.; Nombona, N. Electroanalytical detection of heavy metals using metallophthalocyanine and silica-coated iron oxide composites. *Chem. Pap.* **2018**, *72*, 3043–3056.
- (11) Das, T. R.; Sharma, P. K. Sensitive and selective electrochemical detection of Cd<sup>2+</sup> by using bimetal oxide decorated Graphene oxide (Bi<sub>2</sub>O<sub>3</sub>/Fe<sub>2</sub>O<sub>3</sub>@GO) electrode. *Microchem. J.* **2019**, *147*, 1203–1214.
- (12) Lee, S.; Oh, J.; Kim, D.; Piao, Y. A sensitive electrochemical sensor using an iron oxide/graphene composite for the simultaneous detection of heavy metal ions. *Talanta* **2016**, *160*, 528–536.
- (13) Maleki, B.; Baghayeri, M.; Ghanei-Motlagh, M.; Mohammadi Zonoz, F.; Amiri, A.; Hajizadeh, F.; Hosseini, A.; Esmailnezhad, E. Polyamidoamine dendrimer functionalized iron oxide nanoparticles for simultaneous electrochemical detection of Pb<sup>2+</sup> and Cd<sup>2+</sup> ions in environmental waters. *Measurement* **2019**, *140*, 81–88.
- (14) Wu, W.; Jia, M.; Zhang, Z.; Chen, X.; Zhang, Q.; Zhang, W.; Li, P.; Chen, L. Sensitive, selective and simultaneous electrochemical detection of multiple heavy metals in environment and food using a lowcost Fe<sub>3</sub>O<sub>4</sub> nanoparticles/fluorinated multi-walled carbon nanotubes sensor. *Ecotoxicol. Environ. Saf.* **2019**, *175*, 243–250.
- (15) Chen, Y.; Zhang, D.; Wang, D.; Lu, L.; Wang, X.; Guo, G. A carbon-supported BiSn nanoparticles based novel sensor for sensitive electrochemical determination of Cd(II) ions. *Talanta* **2019**, *202*, 27–33.
- (16) Ouyang, R.; Zhu, Z.; Tatum, C. E.; Chambers, J. Q.; Xue, Z.-L. Simultaneous Stripping Detection of Pb(II), Cd(II) and Zn(II) Using a Bimetallic Hg-Bi/Single-Walled Carbon Nanotubes Composite Electrode. *J. Electroanal. Chem.* **2011**, *656*, 78–84.
- (17) Amare, M.; Worku, A.; Kassa, A.; Hilluf, W. Green synthesized silver nanoparticle modified carbon paste electrode for SWAS

voltammetric simultaneous determination of Cd(II) and Pb(II) in Bahir Dar Textile discharged effluent. *Heliyon* **2020**, *6*, No. e04401.

(18) Hayat, A.; Marty, J. Disposable Screen Printed Electrochemical Sensors: Tools for Environmental Monitoring. *Sensors* **2014**, *14*, 10432–10453.

(19) Wang, H.; Zhao, G.; Yin, Y.; Wang, Z.; Liu, G. Screen-Printed Electrode Modified by Bismuth/Fe<sub>3</sub>O<sub>4</sub> Nanoparticle/Ionic Liquid Composite Using Internal Standard Normalization for Accurate Determination of Cd(II) in Soil. *Sensors* **2017**, *18*, 6.

(20) Li, C.-Y.; Wei, Y.-Y.; Shen, W.; Dong, X.; Yang, M.; Wei, J. Ultrahigh sensitivity electroanalysis of trace As(III) in water and human serum via gold nanoparticles uniformly anchored to Co<sub>3</sub>O<sub>4</sub> porous microsheets. *Electrochim. Acta* **2021**, *368*, 137605.

(21) Sengupta, P.; Pramanik, K.; Sarkar, P. Simultaneous detection of trace Pb(II), Cd(II) and Hg(II) by anodic stripping analyses with glassy carbon electrode modified by solid phase synthesized iron-aluminate nano particles. *Sens. Actuators, B* **2021**, *329*, 129052.

(22) Kyaw, H. H.; Al-Harathi, S. H.; Sellai, A.; Dutta, J. Self-organization of gold nanoparticles on silanated surfaces. *Beilstein J. Nanotechnol.* **2015**, *6*, 2345–2353.

(23) Rao, X.; Guyon, C.; Ognier, S.; Da Silva, B.; Chu, C.; Tatoulian, M.; Hassan, A. A. High density gold nanoparticles immobilized on surface via plasma deposited APTES film for decomposing organic compounds in microchannels. *Appl. Surf. Sci.* **2018**, *439*, 272–281.

(24) Khan, M. Z. H.; Liu, X.; Zhu, J.; Ma, F.; Hu, W.; Liu, X. Electrochemical detection of tyramine with ITO/APTES/ErGO electrode and its application in real sample analysis. *Biosens. Bioelectron.* **2018**, *108*, 76–81.

(25) Amri, S. A. S.; Yusof, N. A.; Abdullah, J.; Rahman, S. F. A.; Azmi, U. Z. M. Enhancement of Electrochemical Properties Using Iron Oxide-Gold Nanocomposite for Tuberculosis Detection Based on rGO-APTES Modified Screen-Printed Electrode. *IEEE Sens. J.* **2021**, *21*, 7233–7241.

(26) Ballarin, B.; Cassani, M. C.; Scavetta, E.; Tonelli, D. Self-assembled gold nanoparticles modified ITO electrodes: The monolayer binder molecule effect. *Electrochim. Acta* **2008**, *53*, 8034–8044.

(27) Ghazali, N. N.; Mohamad Nor, N.; Abdul Razak, K.; Lockman, Z.; Hattori, T. Hydrothermal synthesis of bismuth nanosheets for modified APTES-functionalized screen-printed carbon electrode in lead and cadmium detection. *J. Nanopart. Res.* **2020**, *22*, 211.

(28) Han, T.; Jin, J.; Wang, C.; Sun, Y.; Zhang, Y.; Liu, Y. Ag nanoparticles-modified 3D graphene foam for binder-free electrodes of electrochemical sensors. *Nanomaterials* **2017**, *7*, 40.

(29) Hebbar, R. S.; Isloor, A. M.; Ismail, A. F.; Shilton, S. J.; Obaid, A.; Fun, H.-K. Probing the morphology and anti-organic fouling behaviour of a polyetherimide membrane modified with hydrophilic organic acids as additives. *New J. Chem.* **2015**, *39*, 6141–6150.

(30) Aziz, M. A.; Patra, S.; Yang, H. A facile method of achieving low surface coverage of Au nanoparticles on an indium tin oxide electrode and its application to protein detection. *Chem. Commun.* **2008**, *38*, 4607–4609.

(31) Randles, J. E. B. A cathode ray polarograph. Part II.—The current-voltage curves. *Trans. Faraday Soc.* **1948**, *44*, 327–338.

(32) Ševčík, A. Oscillographic polarography with periodical triangular voltage. *Collect. Czech. Chem. Commun.* **1948**, *13*, 349–377.

(33) Li, W.-J.; Yao, X.-Z.; Guo, Z.; Liu, J.-H.; Huang, X.-J. Fe<sub>3</sub>O<sub>4</sub> with novel nanoplate-stacked structure: Surfactant-free hydrothermal synthesis and application in detection of heavy metal ions. *J. Electroanal. Chem.* **2015**, *749*, 75–82.

(34) Zhou, S.-F.; Han, X.-J.; Liu, Y.-Q. SWASV performance toward heavy metal ions based on a high-activity and simple magnetic chitosan sensing nanomaterials. *J. Alloys Compd.* **2016**, *684*, 1–7.

(35) Ramalingam, M.; Ponnusamy, V. K.; Sangilimuthu, S. N. A nanocomposite consisting of porous graphitic carbon nitride nanosheets and oxidized multiwalled carbon nanotubes for simultaneous stripping voltammetric determination of cadmium(II), mercury(II), lead(II) and zinc(II). *Microchim. Acta* **2019**, *186*, 69.

(36) Eswaran, M.; Tsai, P.-C.; Wu, M.-T.; Ponnusamy, V. K. Novel nano-engineered environmental sensor based on polymelamine/graphitic-carbon nitride nanohybrid material for sensitive and simultaneous monitoring of toxic heavy metals. *J. Hazard. Mater.* **2021**, *418*, 126267.

(37) Manivannan, A.; Kawasaki, R.; Tryk, D. A.; Fujishima, A. Interaction of Pb and Cd during anodic stripping voltammetric analysis at boron-doped diamond electrodes. *Electrochim. Acta* **2004**, *49*, 3313–3318.

(38) Nor, N. M.; Razak, K. A.; Lockman, Z. Glucose-sensing properties of citrate-functionalized maghemite nanoparticle-modified indium tin oxide electrodes. *J. Mater. Res.* **2020**, *35*, 1279–1289.